Journal of MATERIALS RESEARCH

Article
DOI:10.1557/s43578-024-01319-3

Coating of expanded polystyrene spheres by TiO_2 and SiO_2–TiO_2 thin films

Piotr Miądlicki[1,a], Piotr Rychtowski[1], Beata Tryba[1,a]

[1] *Engineering of Catalytic and Sorbent Materials Department, Faculty of Chemical Technology and Engineering, West Pomeranian University of Technology in Szczecin, Pułaskiego 10, 70-322 Szczecin, Poland*

[a] Address all correspondence to these authors. e-mails: piotr.miadlicki@zut.edu.pl; beata.tryba@zut.edu.pl

Received: 28 July 2023; accepted: 28 February 2024

Expanded polystyrene spheres (EPS) were coated by SiO_2–TiO_2 or TiO_2 for application as a fluidized bed in the photocatalytic reactor. Silica coating was realized by the sol–gel process carried out in a vacuum evaporator at 60–70 °C. The most uniform and thin layer of silica coating was obtained by the Stöber method based on the hydrolysis of tetraethyl orthosilicate (TEOS) catalysed by an ammonia solution. Effective TiO_2 coating was obtained by the immersion of EPS in the titania aqueous suspension and evaporation of water in a vacuum evaporator. Heating of EPS spheres coated by SiO_2, TiO_2 or SiO_2–TiO_2 at the temperatures of 120–140 °C resulted in a shrinkage of their volume. For the thick layer coating, a strong corrugation of EPS surface was observed. The photocatalytic tests showed, that highly corrugated surface of coated EPS slowed down ethylene decomposition, whereas a thin layer coating of both, SiO_2 and TiO_2 was advantageous.

Introduction

Recently photocatalytic reactors have been widely studied with the application of the photocatalytic bed, where photocatalyst is coated on the inert support. There are two approaches, the reactors with the stationary bed and fluidized one. Application of reactors with the fluidized bed is highly advantageous for the photocatalytic processes, because of enhanced contact between the photocatalytic bed and irradiating light, while this contact in fixed bed is significantly limited. However, to obtain the fluidization state of bed, higher velocities of flowing gas through the reactor are necessary. With increase a gas flow, the contact time of gaseous molecules with a photocatalytic bed decrease. Photocatalytic decomposition of organic pollutants depends on the mass transfer of substrate to the active sites of the photocatalyst. Therefore, to obtain high yield of the photocatalytic process, the laminar flow of a gas stream through the reactor is necessary. There are some examples of fluidized bed reactors applied for the photocatalytic processes. One of them is a reactor filled with activated carbon coated by TiO_2 (size of 100–150 μm) [1, 2]. The other examples of the photocatalytic beds are: TiO_2-coated silica gel [3], quartz sand [4] or clay granules [5]. Mentioned above support materials for TiO_2 coating, despite of being inert and highly porous, possess high density, which in consequence force the high rates of a gas flow to create the fluid state. The activated carbon seems to be suitable material, because is very light, however, it is also very fragile and highly heterogeneous, what may cause negative effect of bed stacking. From this point of view, the expanded polystyrene spheres (EPS) emerge as the ideal support materials for TiO_2 immobilization, because they are very light, homogenous in shape and easy acquired.

Polymer/inorganic and others composites [6, 7] have been already known and used in many fields e.g., drug release [8], catalysis [9], biochemistry [10] or photocatalysis [11]. Polymer/inorganic composites combine the advantages of both, the organic polymer, which serves as a core (low density, easy for synthesis and processing, ductility) and the inorganic material used as a shell (catalytic activity, thermal and chemical stability, porosity). The most common core/shell composites used are based on the polymer core with a silica shell [12–16]. Such composites can be obtained by several methods. One of the examples is application of polymer spheres coating with nanosilica layer through the sol–gel Stöber method, which involves the synthesis of nanosilica by hydrolysis reaction of silicon alkoxide (most often tetraethyl orthosilicate) catalyzed by ammonia solution. According to this method, the size of silica particles can be readily tuned in a wide range from 10 to 500 nm by simply

altering the ammonia concentration. Silica particles on the polymer surface larger than 250 nm are obtained at higher ammonia concentrations [12, 17]. The hydrolysis of silicon alkoxide can also be carried out at the presence of hydrochloric acid used as a catalyst. The thickness of the silica layer is strongly dependent on the pH solution and reaction time. As the pH of the reaction mixture decreases, the silica layer becomes thicker, that gives the possibilities to obtain a layer of precise thickness [13]. Additionally, the pore size of the silica coating can be modified by adding a surfactant during the synthesis process. The mesoporous silica with an ordered structure can be obtained by addition of the Pluronic P123 or cetyltrimethylammonium bromide (CTAB) surfactants [18–20]. The physical method of composites preparation comprises of mixing opposite charged particles and then processing them into more regular structures by melting. Such method is much faster, cheaper and generates much less harmful waste [21–23]. Another method of fixing an inorganic layer to a polymer core is using the coating slurry and evaporating the solvent [24]. This allows to obtain an inorganic layer with strictly defined properties without significant interference with the coated material.

Various pretreatment methods are used to increase the affinity of the polymer to the inorganic layer. One of them is modification of the polymer surface with a coupling agent e.g., poly(vinylpyrrolidone). It affects the stability of colloids as well as the homogeneity and smoothness of the initial silica coating [25]. Effective coating of the polymer surface with an inorganic layer can be also achieved by increasing a polymer hydrophilicity, which results in the increase of the oxygen groups on its surface. For this purpose, the polymer surface can be modified by UVC radiation [26], plasma [27, 28] or chemical treatment [29, 30].

Some methods of TiO_2 or SiO_2 coating EPS have been described in the literature. One of the example is physical vapour deposition of SiO_2 and TiO_2 films on the non-expanded polystyrene beds, which were then expanded and molded into a one piece of polystyrene foam [31]. Another example is dissolving of EPS surface in acetone solution with immobilization of TiO_2 particles [32]. The method of TiO_2 grafted EPS through the polystyrene solution and ethyl acetate was also reported [32]. Some thermal methods of TiO_2 particles embedding into the EPS structure can be utilized, based on the temperature of polystyrene melting, which was estimated to be around 140–150 °C [23, 33, 34].

The aim of this work was to obtain composites made of a polystyrene core and an inorganic SiO_2–TiO_2 bilayer. The studies have been also focused on EPS coating by TiO_2 only. Two different titania materials were applied for EPS coating to analyze the impact of TiO_2 properties on the formation of titania layer.

Expanded polystyrene spheres were used, because of their extremely low bulk density. Silica interlayer was applied to protect polystyrene against degradation at the presence of UV light irradiation [35]. Although the depth of UV penetration in TiO_2 is not so high [36], polystyrene spheres can undergo photocatalytic degradation in the case of a very thin layer of direct TiO_2 coating.

Results

Coating of EPS with SiO_2

SEM images of unmodified EPS spheres and those covered with silica using various methods are illustrated in Fig. 1.

The diameter of the uncoated EPS spheres was in the range of 1.1 to 1.4 mm [Fig. 1(a)]. It can be observed that SiO_2 coating using CTAB surfactant led to the formation of a thick layer of silica, which peeled off the sphere surface [Fig. 1(b)]. Moreover, individual spheres stuck to each other, and the silica coating was not uniform. In [Fig. 1(c)] there are shown EPS spheres coated SiO_2 in the method of TEOS hydrolysis in HCl solution. Moreover, the silica layer obtained in this way was in the form of small flakes outstanding from the EPS surface. The best coverage of the EPS spheres with the silica layer was obtained by the Stöber method [Fig. 1(d)]. The obtained layer of silica was uniform, and all the spheres seem to be almost entirely coated. This method was selected for the further studies due to the good properties of the obtained coating. In the next step the quantity of NH_4OH solution added to the reaction mixture during TEOS hydrolysis was varied.

In Fig. 2 there are showed SEM images of EPS spheres coated by SiO_2 with using a Stöber method and varied amount of ammonia solution.

In these SEM images can be observed increase the silica particle size (from 109.9 ± 10.1 to 184.6 ± 24.5 nm) with increasing the ammonia concentration. Moreover, higher concentration of ammonia solution favors formation of a more uniform layer of silica. In Fig. S1 (Supplementary materials) there are illustrated SEM–EDS images of EPS spheres coated with SiO_2 using 0.5 and 1.5 ml NH_4OH.

At the presence of higher ammonia concentration, the thickness of SiO_2 coating seems to be lower. EDS analyses indicated, that for 1.5 ml NH_4OH used, the quantity of Si on EPS spheres was equaled around 2.5% atom, whereas for 0.5 ml ammonia solution it was around 4% atom.

Size distribution of SiO_2 particles obtained from TEOS hydrolysis by a Stöber method and zeta potential

Synthesis of SiO_2 via sol–gel method from TEOS, ethanol and ammonia solution were performed to analyze impact of ammonia solution on the homogeneity of hydrolyzed SiO_2 particles. The conditions of sol–gel process were identical as those used for EPS spheres coating. The measurements of SiO_2 particles size

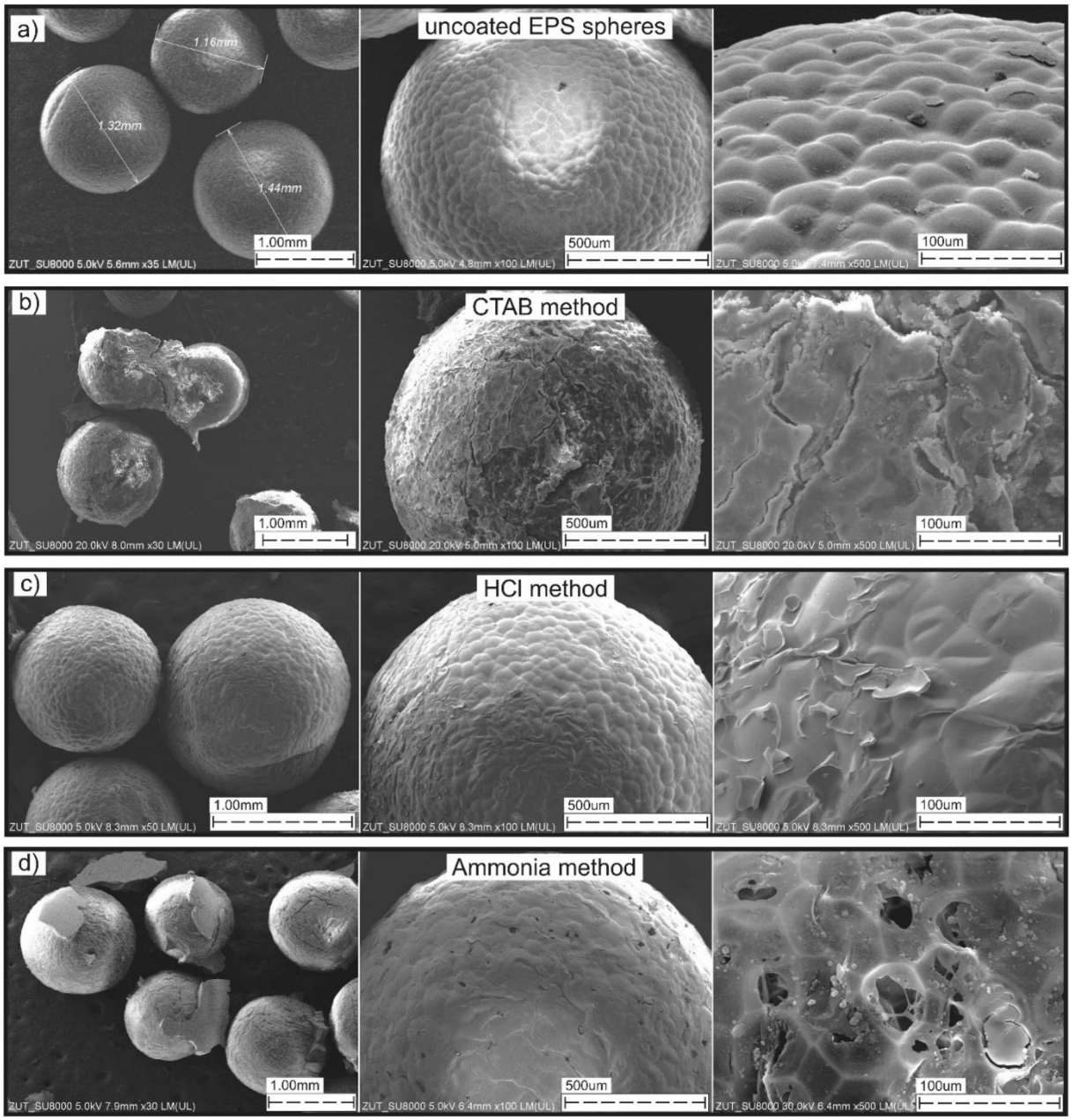

Figure 1: SEM images of EPS spheres: uncoated (a); coated SiO_2 from the sol–gel solution using different conditions: CTAB surfactant (b), HCl solution (c), and NH_4OH solution (d).

were performed by Dynamic Light Scattering (DLS) method in Zetasizer Nano ZS apparatus of Malvern company (UK). Obtained in a sol–gel method SiO_2 powder was simply dispersed in the deionized water mixed, and then analyzed.

Lack of ammonia solution or its little content (0.5 ml) caused formation of SiO_2 particles with bimodal distribution (80 nm and 200 nm). Higher volume of ammonia solution added to sol–gel mixture caused precipitation of higher size silica particles with more narrow size distribution (150–200 nm). It was concluded, that at the presence of higher ammonia concentration used during SiO_2 synthesis, obtained suspension was more homogeneous. Therefore, in a further step of EPS-SiO_2–TiO_2 synthesis, the Stöber method of silica coating with addition of 1.5 ml NH_4OH was used. Particles size distribution (by light intensity) obtained at the presence of various quantity of ammonia solution used during SiO_2 synthesis is shown in Fig. S2 (Supplementary materials).

Measurements of zeta potential for SiO_2 particles indicated, that addition of ammonia to sol–gel solution during silica synthesis increased negative charge of SiO_2 particles, without

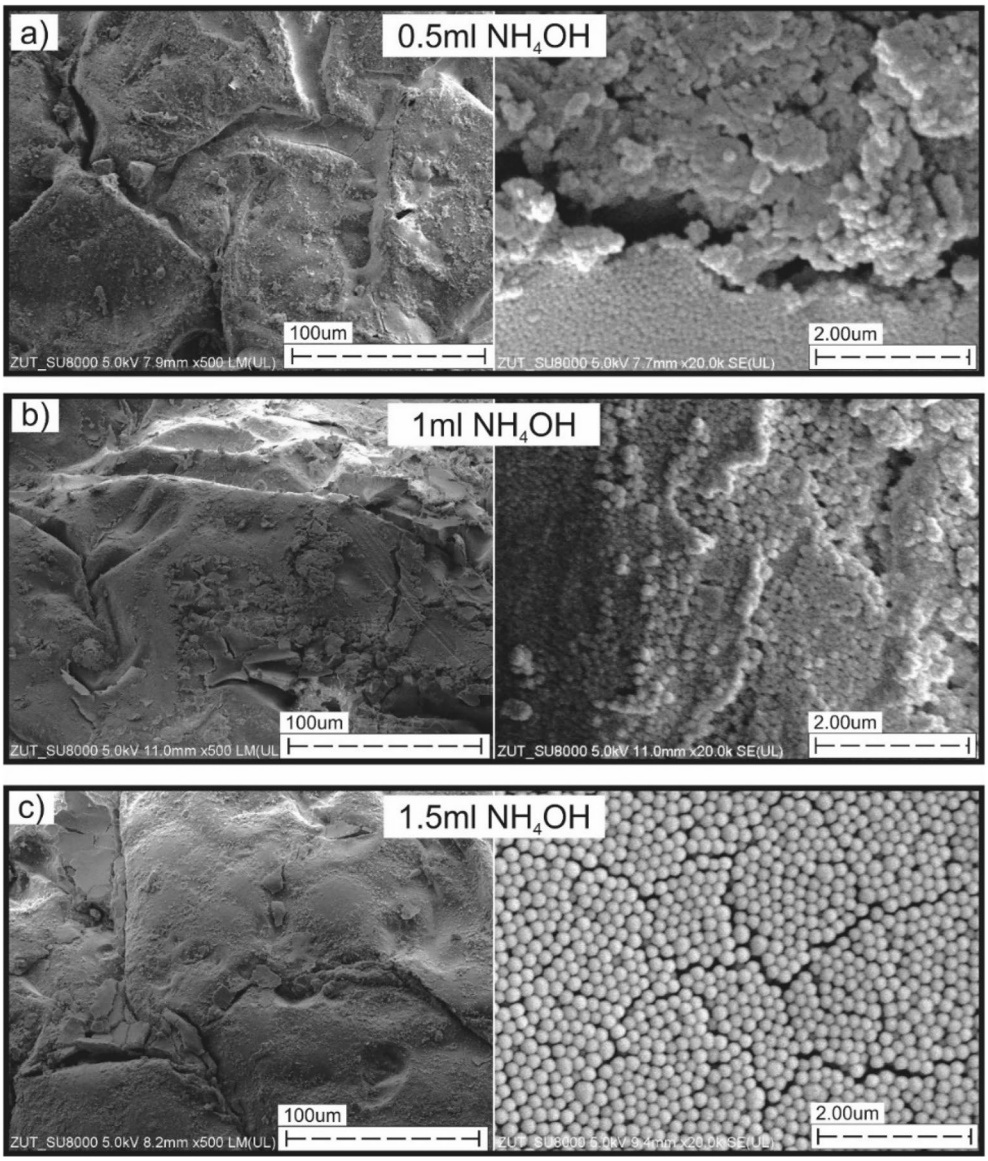

Figure 2: SEM images of EPS spheres coated with SiO_2 from the sol–gel solution at the conditions of different NH_4OH dosing: (a) 0.5 ml, (b) 1 ml, and (c) 1.5 ml.

ammonia was equaled (– 25 mV), at the presence of 0.5 ml NH_4OH decreased to (– 30 mV), but after addition of 1.5 ml dropped down to (– 33 mV).

Coating of EPS with SiO_2–TiO_2

EPS spheres coated by SiO_2 were submitted to coating with another layer, i.e., TiO_2, which was realized by two methods. The first one was based on the TIPOT hydrolysis conducted directly onto EPS-SiO_2 spheres. However, obtained in this way TiO_2 coating was not uniform, some agglomerates of TiO_2 particles on the spheres surface with poor abundance were observed [Fig. 3(a)]. The second method used was based on coating of EPS-SiO_2 by a crystalline TiO_2 from its aqueous suspension. For that purpose, two different TiO_2 materials were utilized, commercial (P25, Evonik, [Fig. 3(b)]) and the other one, obtained in the laboratory, marked as Ar400 [Fig. 3(c)]. In case of TiO_2-P25 a thick and rather flat layer of coating is observed, but for the other TiO_2 sample (Ar400), the coating surface is rough, although titania did not entirely cover the outer surface of EPS-SiO_2 spheres.

Thermal treatment of EPS-SiO_2 composites

EPS-SiO_2 composites prepared by TEOS hydrolysis (Stöber method, 1.5 ml NH_4OH) were submitted to the thermal treatment at 120–140 °C in an oven for 6 h in order to increase

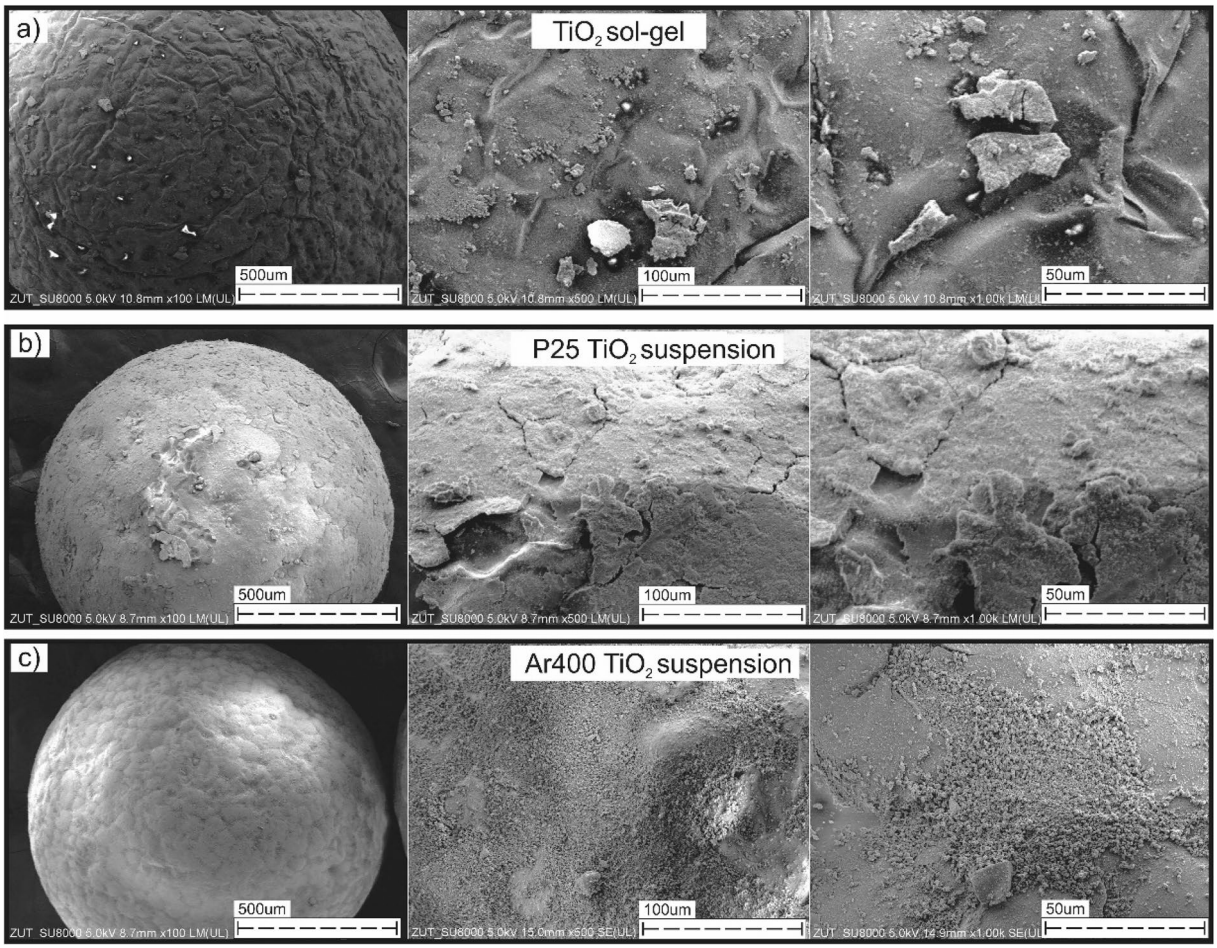

Figure 3: SEM images of EPS-SiO_2 spheres coated with TiO_2 by: (a) TIPOT hydrolysis, (b) and (c) titania aqueous solution: P25 and Ar400, respectively.

adhesion of a coating layer with the polystyrene substrate. Thermal process caused a strong corrugation of the polystyrene surface.

After heating process, the size of the EPS coated SiO_2 spheres was significantly reduced in comparison with the uncoated EPS. The outer layer of EPS surface collapsed, and the obtained composites were shrunk about half of their primary size, however, they preserved their spherical shape with corrugated outline.

In Fig. 4 the SEM images of EPS-SiO_2 spheres heat-treated at 140 °C are shown, in addition the SEM images of EPS-SiO_2 spheres heat-treated at 120 °C are shown in Fig. S3 (Supplementary materials).

At higher temperature of heat-treatment the changes in EPS-SiO_2 structure were more pronounced, the obtained surface was more corrugated, and the spheres look to be more shrunk. Additionally, these SEM images showed some of the silica particles embedded into the polystyrene substrate. The size of SiO_2 particles increased with increasing temperature of heat treatment.

Thermal treatment of EPS-SiO_2–TiO_2 composites

The prepared EPS-SiO_2–TiO_2 spheres were heated at 140 °C, likewise EPS-SiO_2. Changes in their surface morphology after thermal treatment are analyzed by SEM images (Fig. 5).

Heat-treatment of EPS spheres coated with SiO_2–TiO_2 bilayer at 140 °C caused significant reduction of their size, however, the morphology of the coated surface varied by type of TiO_2 used for coating. In case of commercial P25 the coated layer was highly disrupted as opposite to Ar400.

EPS spheres compose of large air spaces inside and most likely the outer layer of coating collapsed due to the increased gas pressure after heating. Laboratory prepared TiO_2 sample Ar400 was highly porous and blended in the silica layer as outstanding powder whereas P25 coated EPS-SiO_2 created rather smooth and thick layer (Fig. 3). Heating of EPS at 140 °C resulted in the decomposition of some polymer ingredients and formed gases imprisoned inside the EPS shell destroyed the outer layer of TiO_2, which was poorly permeable for gases [Fig. 5(a)]. SEM images of EPS spheres in a cross section are

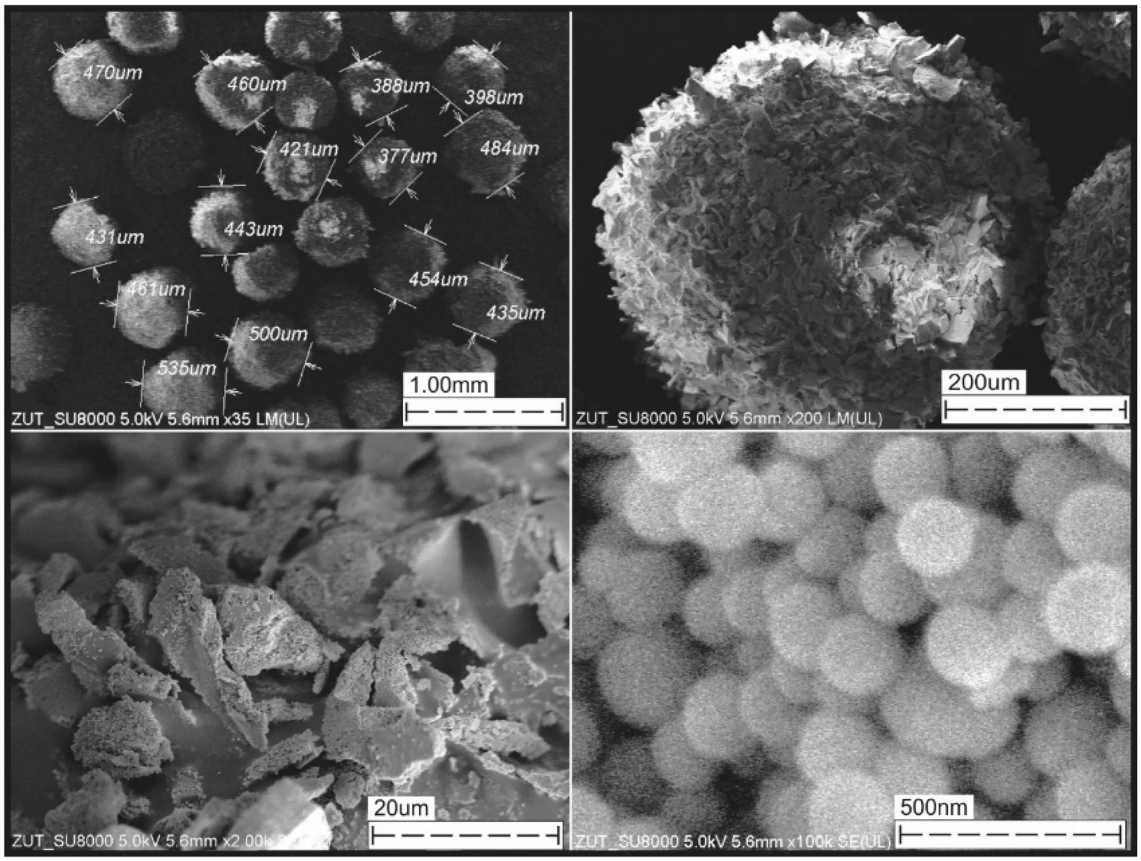

Figure 4: SEM images of EPS-SiO_2 spheres after heating at 140 °C.

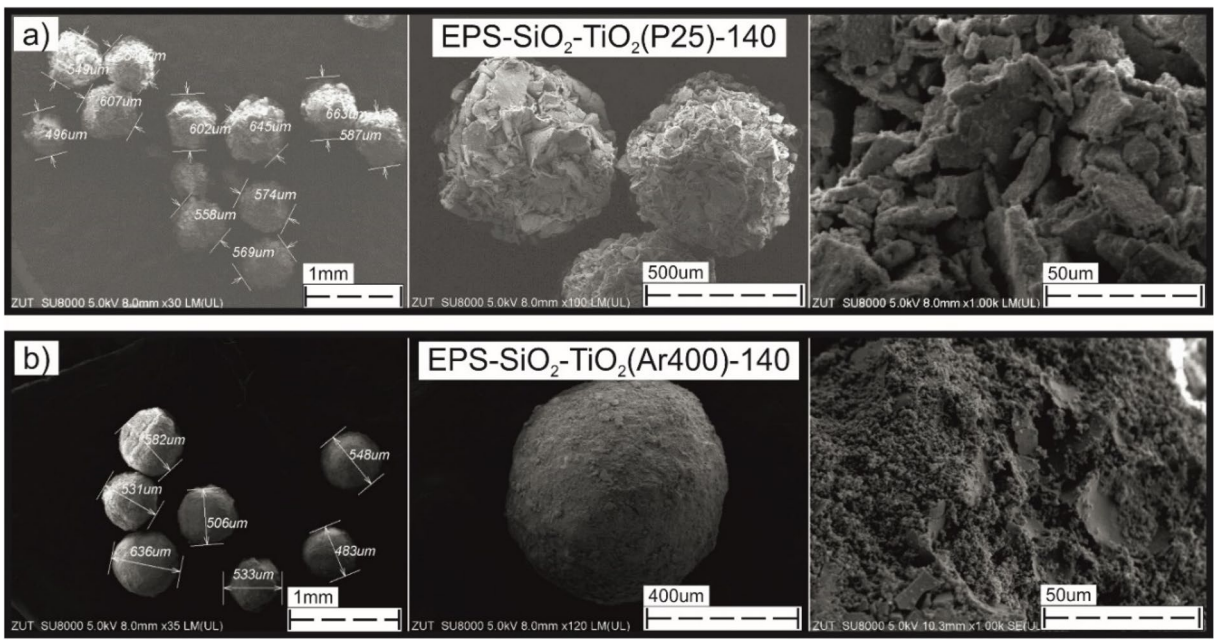

Figure 5: SEM images of EPS-SiO_2–TiO_2 spheres heat-treated at 140 °C, (a) TiO2-P25, (b) TiO_2-Ar400.

shown in Fig. S4 (Supplementary materials). The cross-section shows large cavities inside EPS spheres, which are surrounded by a thin and porous polymer layer. Performed experiments indicated, that the bald EPS spheres without any coating heat-treated at 140 °C shrank a half, but their spherical shape remained without any changes in the surface roughness.

Coating of EPS spheres by impregnation with TiO_2 and following thermal treatment

In the next step EPS spheres were coated by only one layer of TiO_2. The applied method of coating was based on the immersion of EPS spheres in the aqueous suspension of TiO_2 in a rotary evaporator, mixing and then evaporation of water. Evaporation of water proceeded at the temperature of 60–70 °C, because at higher temperature the EPS spheres started to stick to each other, due to the polymer softening. General purpose polystyrene has a softening point at the temperatures range of 75–85 °C [37]. However, in case of low-density EPS spheres with a thin and porous surface this softening can occur at lower temperature. Such impregnated EPS spheres were dried at 70 °C. In Fig. 6 SEM images of EPS-TiO_2 spheres are shown.

The structure of TiO_2 coating differed for both samples, in case of P25 some of the titania conglomerates can be observed whereas Ar400 formed a flaky titania layer. In both cases titania coating of EPS surface was not complete. Measurements of EPS-TiO_2 spheres diameters indicated, that these coated by P25 had higher size than those coated by Ar400. It can be assumed, that P25 coated EPS spheres with somewhat thicker layer than Ar400.

Analyses of TiO_2 distribution on EPS spheres were performed by EDS technique. SEM/EDS images of EPS-TiO_2 spheres are illustrated in Figs. S5 and S6 (Supplementary materials). EDS analyses indicated that titania was not evenly distributed on the EPS spheres. In case of P25 some hollow spaces are observed (Fig. S5), most likely a thick layer of P25 was partly broken away from the EPS surface. Such phenomenon was not observed in case of titania Ar400 (Fig. S6).

Prepared EPS-TiO_2 spheres were submitted to thermal treatment at 140 °C in air. The changes of EPS-TiO_2 structure after heating are depicted in the SEM images (Fig. 7).

The surface structure of EPS-TiO_2 coated by P25 and heated at 140 °C was highly disrupted whereas in case of Ar400 coating was just slightly corrugated. Such huge differences in the structure were caused by diverse properties of these two TiO_2 samples. TiO_2-Ar400 was highly porous and coated EPS spheres with a thin layer, whereas P25 formed a thick and compact layer of titania on the EPS surface. The observed effect was similar to the titania coating of EPS-SiO_2 spheres, described (Fig. 4). Distribution of TiO_2 on the EPS surface was analyzed by EDS technique and is shown in Fig. S7 (Supplementary materials).

Performed EDS analyses showed quite good and even distribution of titania particles on the EPS surface. It is assumed, that heating of EPS-TiO_2 spheres increased adhesion of titania particles to the polymer surface. Shrinkage of EPS spheres resulted in the increasing the quantity of TiO_2 distributed onto the polystyrene surface.

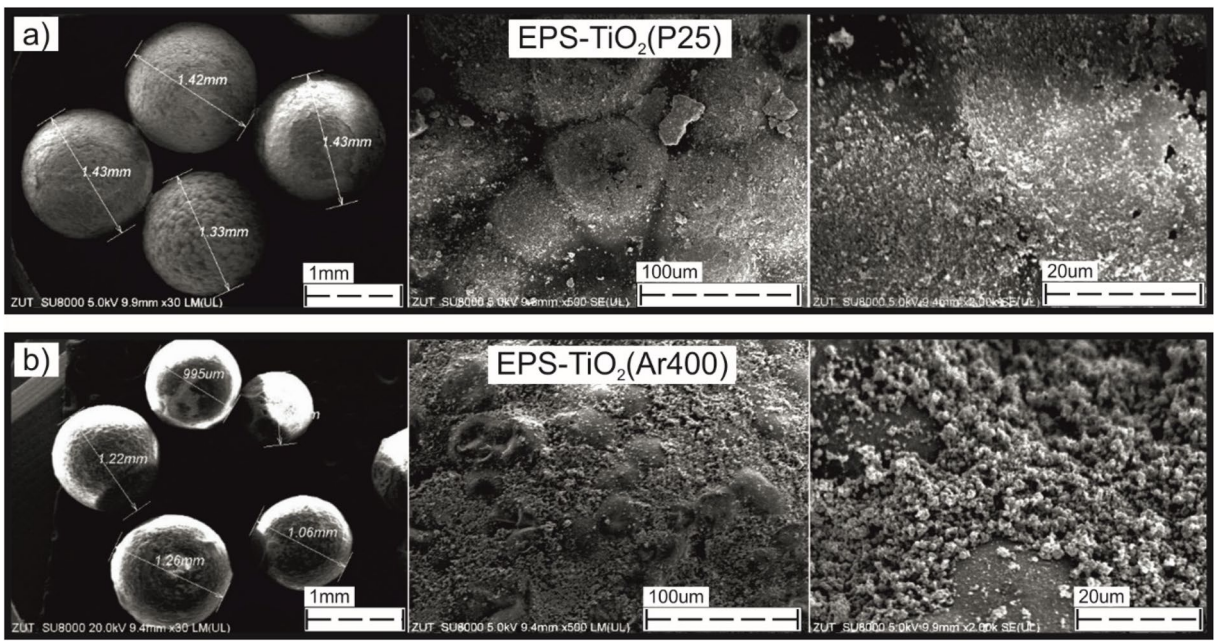

Figure 6: SEM images of EPS-TiO_2 spheres, (a) TiO_2-P25, (b) TiO_2-Ar400.

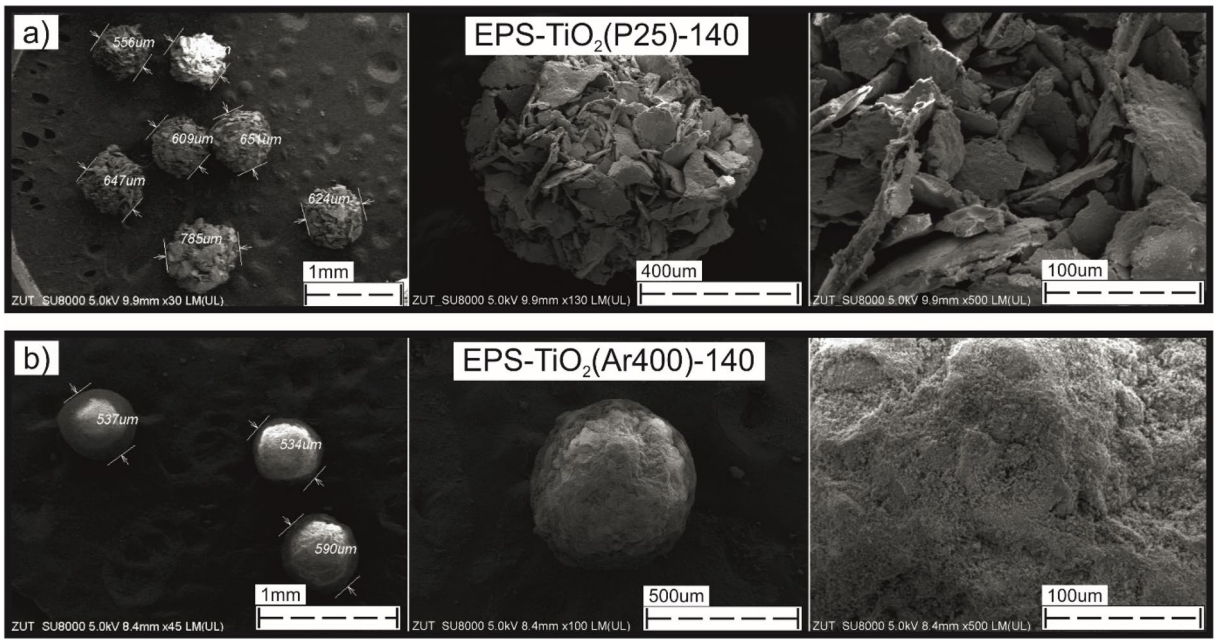

Figure 7: SEM images of EPS-TiO_2 spheres heat-treated at 140 °C, (a) TiO_2-P25, (b) TiO_2-Ar400.

Optical properties of EPS-TiO_2 and EPS-SiO_2–TiO_2 composites

The measurements of UV–Vis absorption for EPS-TiO_2 and EPS-SiO_2–TiO_2 composites as prepared and heat-treated at 140 °C were performed. For comparison the UV–Vis spectra of EPS spheres as well as TiO_2 and SiO_2 powders were also added. All the recorded UV–Vis spectra are presented in Fig. 8.

EPS spheres showed insignificant absorption of light in the visible range. Coating of EPS spheres by amorphous silica did not cause any spectacular changes in the UV–Vis spectrum [Fig. 8(a)]. TiO_2-Ar400 indicated slight absorption of visible light in the range of 400–500 nm, contrary to P25. Both TiO_2 samples absorbed UV light, however, in case of P25 the absorption edge was slightly shifted to the higher wavelengths. This was caused by the composition of P25, which contained around 22 wt% of rutile. Rutile has a lower energy of the band gap than anatase, so can absorb light at the visible range (390–415 nm). In addition, photocurrent response measurements were performed under irradiation of 388 nm wavelength (Fig. S8), which showed about 4 times more current generated in the case of TiO_2-Ar400 compared to TiO_2-P25, demonstrating the superiority of the former. Furthermore, TiO_2-P25 showed a significantly higher impedance (Fig. S9) compared to TiO_2-Ar400, as measured by electrochemical impedance spectroscopy (EIS). These properties could impact the overall photocatalytic properties of studied samples.

Heating of EPS composites at 140 °C resulted in both, shifting the UV–Vis spectra to the higher wavelengths and increase of visible light absorption. Heat-treatment of EPS spheres at 140 °C caused their slow degradation and formed byproducts were diffused through the coating layer and adsorbed on their surface. EPS composites after heating revealed changes in color from white onto yellowish and brown. This effect was more pronounced in case of a thin layer coating (TiO_2-Ar400). Formation of rough surface with large, opened cavities in case of P25 coating conducted to higher harvesting of visible light—effect related to the 3D structure (UV–Vis spectrum for EPS-TiO_2(P25)-140, [Fig. 8(c)]).

The plots of Kubelka–Munk function versus energy are depicted in Fig. S9 (Supplementary materials). For powdered P25 two band gap values were observed, for anatase (3.16 eV) and rutile (2.97 eV), due to its mixed phase composition. However, coating of P25 onto polystyrene surface made some difficulties in separation of these two band gaps. Therefore, the band gap determined for P25 in composites is a combination of anatase and rutile and is as follows EPS-P25 = 3.06; EPS-SiO_2-P25 = 3.08). Heat treatment of EPS coated with P25 at 140 °C did not result in a band gap shift and is equal to 3.04. TiO_2-Ar400 sample consisted mainly of anatase and revealed a band gap value of 3.19 eV. Heat-treatment of EPS coated with TiO_2 (Ar400) at 140 °C resulted in the increasing of its band gap energy to 3.26 eV, due to the presence of some carbon impurities, descendent from EPS degradation.

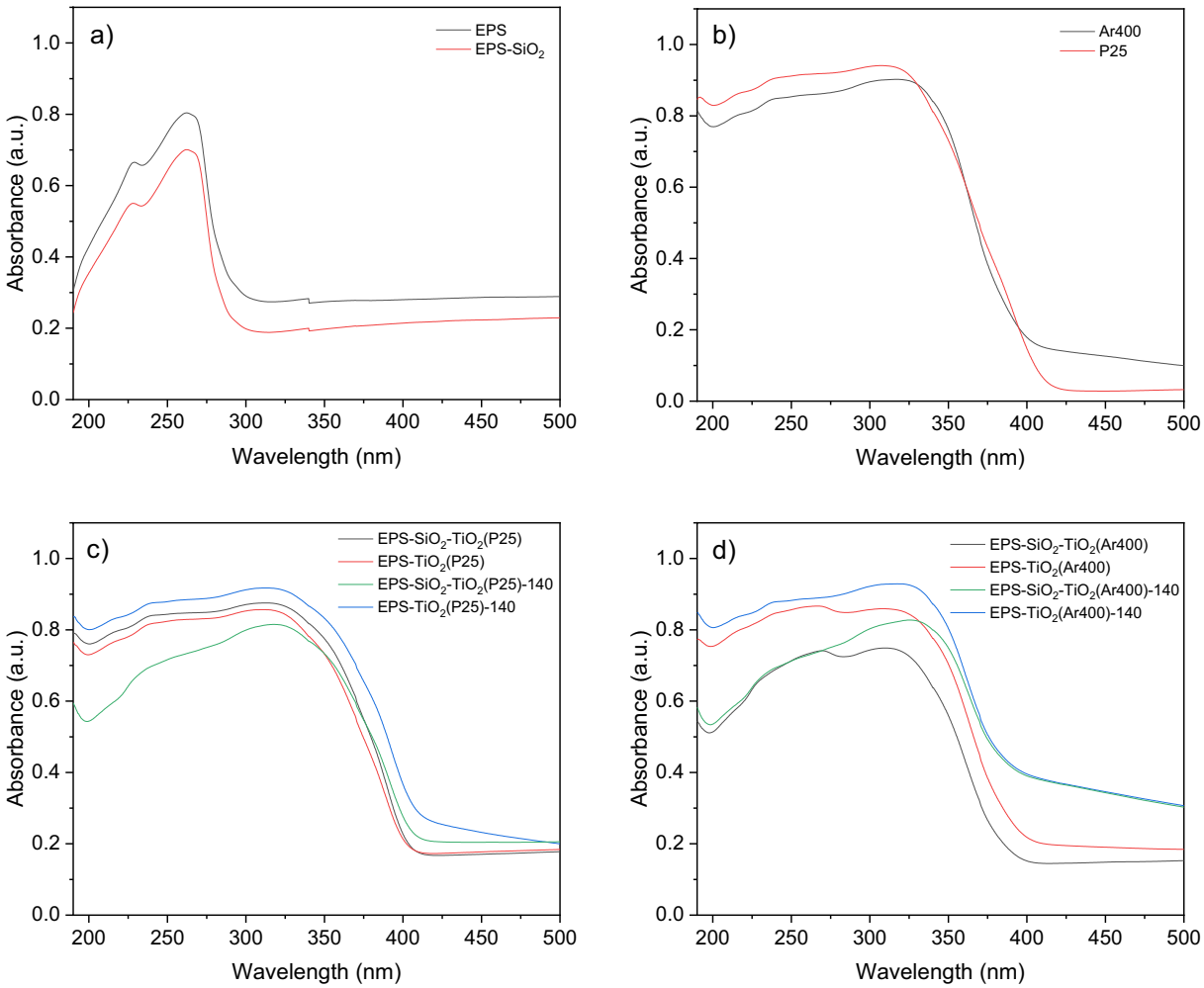

Figure 8: UV–Vis spectra of (a) EPS spheres: unmodifed and SiO_2 coated, (b) TiO_2 samples used for coating, (c) EPS coated by TiO_2 P25 and SiO_2–TiO_2 as received and after heating at 140 °C and (d) EPS coated by TiO_2 Ar400 and SiO_2–TiO_2 as received and after heating at 140 °C.

Thermogravimetric analyses

Thermogravimetric (TG) analyses were performed to determine the mass contents of TiO_2 and SiO_2 in EPS composites. In Fig. S10 (Supplementary materials) there are presented obtained TG curves from thermal decomposition of EPS, EPS-SiO_2 and EPS-SiO_2–TiO_2(Ar400) as an example. Drop in mass during heating of these composites resulted from the combustion of EPS spheres, whereas SiO_2 and TiO_2 leftovers remained in the crucible. In Fig. 8 there are collected data of SiO_2 and TiO_2 contents in different prepared composites with EPS spheres.

Figure 9(a) shows the mass content of SiO_2 in EPS-SiO_2 composites obtained via TEOS hydrolysis conducted at the presence of ammonia solution and EPS spheres. These results revealed that the quantity of SiO_2 was the highest at the conditions of low dose of NH_4OH addition (0.5 ml) and was decreasing with increase ammonia concentration. Most likely ammonia species improved dispersion of silica particles in a sol–gel solution and caused, that SiO_2 coating was in the form of a thin and more homogeneous layer. Coating of EPS spheres by TiO_2 from the titania aqueous suspension resulted in the surface coverage of 27–29 wt%, little higher for P25 sample than Ar400 [Fig. 9(b)]. However, coating of EPS-SiO_2 spheres with TiO_2 was more effective in case of Ar400 with the quantity of around 27 wt% [Fig. 9(c)]. Amount of P25 coated on EPS-SiO_2 was less than 20 wt%. Sol–gel method used for coating titania on EPS-SiO_2 spheres appeared to be less effective, with score of 8 wt% coated TiO_2 only.

These measurements showed that coating of TiO_2(Ar400) on the silica layer was the same effective than that on EPS spheres, but in case of P25 much lower quantity of TiO_2 was deposited on silica than EPS surface. Such difference was caused by the other properties of these two titania samples, Ar400 had higher quantity of hydroxyl groups than P25 [38], so exhibited higher affinity to the silica surface.

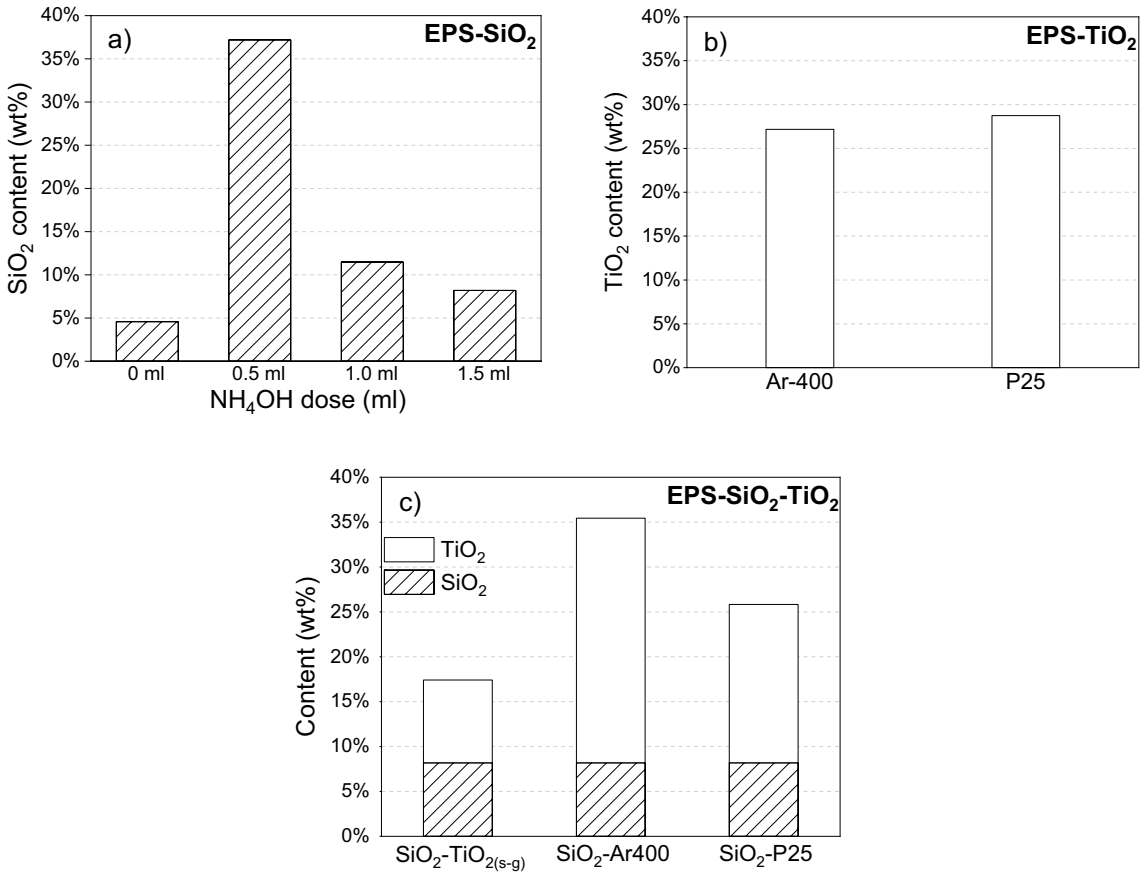

Figure 9: Mass content of SiO_2 and/or TiO_2 by TG analyses in: (a) EPS-SiO_2, (b) EPS-TiO_2 and (c) EPS-SiO_2–TiO_2.

Photocatalytic activity of EPS-TiO_2 and EPS-SiO_2–TiO_2 composites

Prepared composites with EPS spheres were tested for the photocatalytic decomposition of ethylene under UV light irradiation. Photocatalytic process was carried out under continuous flowing of a gas stream through the reactor with a flow rate of 20 ml/min and ethylene concentration of 50 ppm in a synthetic air. These studies were used for comparison of the photocatalytic properties of obtained photocatalytic bed as the preliminary selection of the best material and method of coating. EPS spheres coated with the photocatalytic material were placed on the bottom of the quartz reactor as a single layer, however, for the future application they will be used as a fluidized bed. The results obtained from the photocatalytic tests are presented in Fig. 10.

High photocatalytic activity of TiO_2(Ar400) can be observed by comparison with P25 and TiO_2 obtained from a sol–gel method. Such good activity of Ar400 (100% of ethylene removal) results rather from its physicochemical properties than the quantity of coating. In case of P25 the efficacy of ethylene removal was higher for the obtained EPS-TiO_2 and EPS-SiO_2–TiO_2 spheres without thermal treatment. Highly disrupted structure of EPS coated with P25 after heating at 140 °C resulted in deterioration of its photocatalytic activity. This could be caused by hindered diffusion of ethylene species to the highly disordered and rough TiO_2 surface. Slower rate of ethylene decomposition was also observed for Ar400 coatings after heating of EPS-TiO_2 and EPS-SiO_2–TiO_2 spheres at 140 °C, however, in the case of this sample the outer surface was smoother, so the deterioration of the photocatalytic activity was negligible.

Cyclic test of studied composite photocatalytic activity was conducted in order to study its reusability. Composite EPS-TiO_2(Ar400) was used in this test. The results of the test is presented in Fig. S11 (Supplementary materials). No decrease in photocatalytic activity was observed after three cycles of the process. Performed test prove that the obtained composites are stable and can be used repeatedly and continuously.

The effect of ethylene adsorption on selected composites is also studied (Fig. S12) (Supplementary materials). EPS-TiO_2(Ar400) and EPS-TiO_2(Ar400)-140 composites were compared. Because of the general, poor ethylene adsorption on TiO_2, tests were performed in the flow of 5 ml/min (instead of 20 ml/min applied in photocatalytic tests). The test on an empty reactor

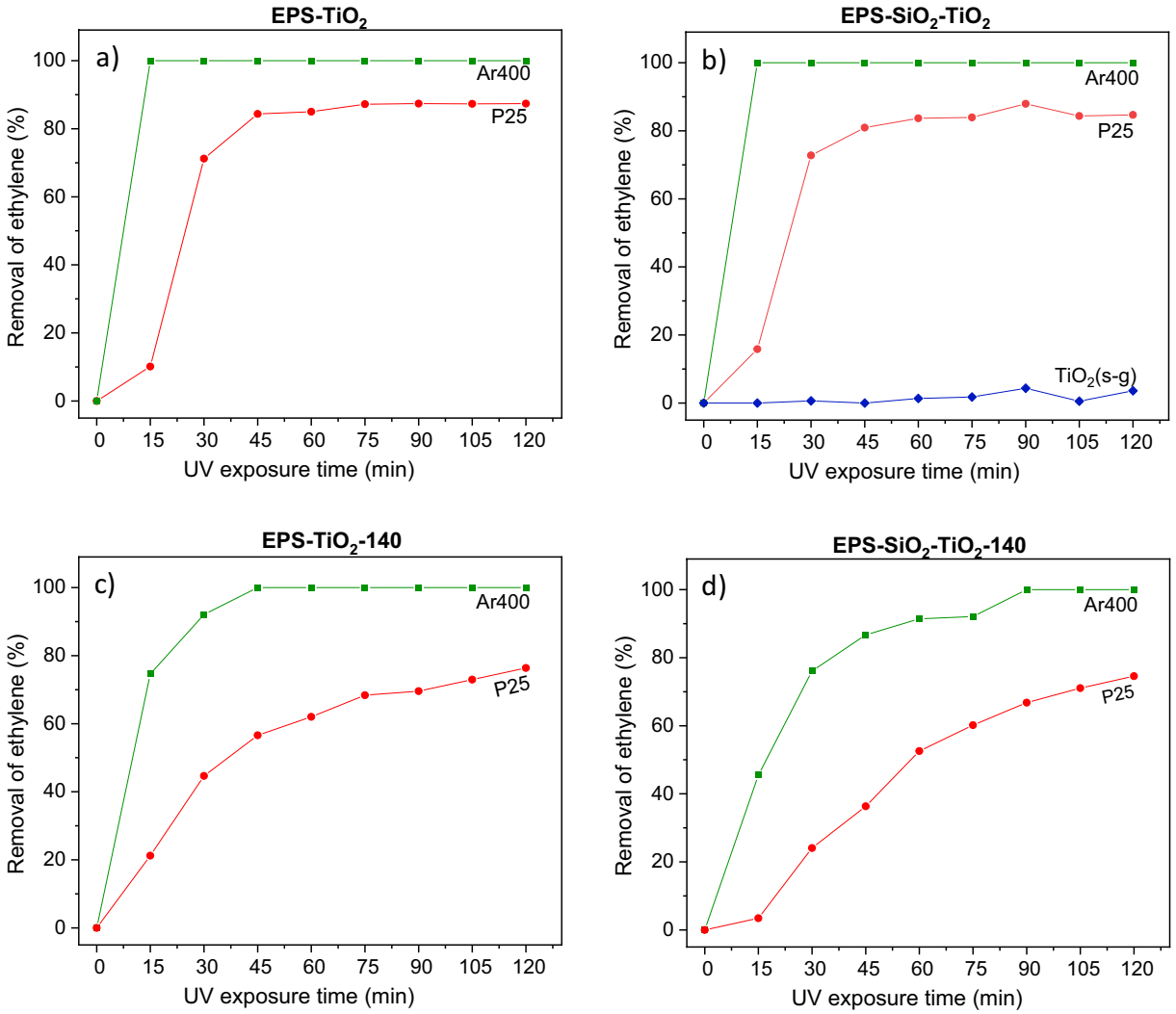

Figure 10: Photocatalytic decomposition of ethylene gas on the (a) EPS coated by TiO_2 P25 or Ar400, (b) EPS coated by SiO_2 and various TiO_2 (P25, Ar400 and TiO_2 prepared by sol–gel method), (c) EPS coated by TiO_2 P25 or Ar400 and heated at 140 °C and (d) EPS coated by SiO_2 and TiO_2 P25 or Ar400 and heated at 140 °C.

was also conducted in order to subtract the effect of background adsorption. The obtained values of ethylene adsorption was comparable and equal to 0.10 μg/cm^2 and 0.09 μg/cm^2 in case of EPS-TiO_2(Ar400) and EPS-TiO_2(Ar400)-140, respectively.

Discussion

These studies showed some possibilities of EPS spheres coating by TiO_2 or SiO_2–TiO_2 for application as the photocatalytic bed in the fluidized bed reactor. EPS coating by TiO_2 can be easily realized through the impregnation method from the titania aqueous suspension in a rotary evaporator with evaporation of water at the temperature of 60–70 °C, close to the border of EPS softening point. However, such TiO_2 coating should be focused on the attachment of a thin layer, because too thick layer can be easily peeled off from the EPS surface. Therefore, selected TiO_2 should have relevant properties, allowing to obtain a good aqueous dispersion and finally should form a porous and thin layer on the EPS surface. Furthermore, when comparing two different TiO_2 used for coating, TiO_2 (Ar400) was more suitable than TiO_2 (P25) because its specific surface area was about 3 times higher than the latter. In fact, SEM images confirmed the higher porous structure of TiO_2 (Ar400) than TiO_2 (P25). It was highly plausible that the aforementioned properties could influence the photocatalytic performance of TiO_2-based composites. Crystalline TiO_2 should be used, because crystallinity of TiO_2 has an impact on the photocatalytic properties of TiO_2 and this impregnation method does not allow to use high temperature of heating for titania crystallization. In case of EPS coating by silica, amorphous structure can be used. Amorphous SiO_2 has high porosity and can increase amount of TiO_2 loading as the

second layer. SiO_2 coating can be successfully realized from the sol–gel solution via Stöber method. The SiO_2 obtained by this method had a relatively high BET surface area (40 m^2/g) and pore volume of 0.22 cm^3/g, which could enhance the loading of TiO_2 onto the composite surface compared to bare EPS spheres. However, for SiO_2 coating a good dispersion of silica particles should be obtained through the controlling of the ammonia concentration. Heating of EPS coated composite with SiO_2, TiO_2 or bilayer SiO_2–TiO_2 at 140 °C caused embedded of SiO_2/TiO_2 particles into the polymer surface, and at this temperature EPS underwent decomposition. As a consequence, heated EPS spheres were shrunk and exposed disrupted surface. Such obtained EPS structure exhibited enhanced absorption of visible light, however appeared to be disadvantageous for application as a photocatalytic bed for removal of gaseous ethylene, because highly corrugated surface hindered diffusion of the gaseous molecules to the active TiO_2 surface. Less disrupted structure of coated EPS heated at 140 °C can be obtained, when it is coated with a thin and porous layer. Generally, the adsorption of ethylene on TiO_2 is poor, which was already proved in our previous studies [38]. It appears that the adsorption of ethylene is not critical in its photocatalytic decomposition process, but its diffusion rate to the photocatalyst surface is. Some studies suggest [39] that TiO_2 surface is activated after light irradiation of its surface. Therefore, the adsorption effect of ethylene can be different under dark and UV light irradiation conditions. The photocatalysis and adsorption processes of ethylene should be treated simultaneously. Therefore, it is stated that the most decisive influence on the photocatalytic decomposition of the ethylene has the formation of radicals and reactive oxygen forms.

Conclusions

EPS spheres can be effectively coated by either TiO_2 nor SiO_2–TiO_2 bilayer. There was proposed a very easily and ecological method of titania coating (without using any solvents) such as impregnation of crystalline TiO_2 from an aqueous suspension in a rotary evaporator with subsequent evaporation of water and then drying at 70 °C. Although this method does not guarantee the total coverage of EPS spheres, the obtained coating layer exhibited high photocatalytic activity by comparison with a sol–gel method, in which poorly crystalized TiO_2 was precipitated. To protect EPS surface from degradation after exposition to UV, coating with silica layer is highly recommended. These studies showed that EPS coating by silica can be successfully realized through the sol–gel process with using Stöber method. Coating of TiO_2 on indirect silica layer was the same effective than directly on EPS spheres in case of TiO_2 (Ar400), however less effective in case of TiO_2 (P25). Such difference was caused by the other properties of these titania samples, Ar400 had higher quantity of hydroxyl groups than P25 [38], so exhibited higher affinity to the silica surface. High surface area and anatase structure of Ar400 were also advantageous features for its application as coating material. Conglomeration of TiO_2 particles on EPS surface (as it was observed in case of P25) conducted to a thick layer coating, which easily peeled off from the surface. It was proved, that heating of EPS composites at the temperatures of 140 °C caused incorporation of SiO_2 or TiO_2 into the EPS structure. However, heat-treatment OD coated EPS spheres resulted in formation of disrupted structure, which had disadvantageous impact on their photocatalytic properties towards ethylene decomposition. In case of anatase type TiO_2 (Ar400) used for EPS coating, the changes in the surface structure of EPS-TiO_2 after heating at 140 °C were insignificant and its photocatalytic properties were quite comparable with unheated composite. In case of the other type of TiO_2 such as commercially produced P25, large irregular cracks were formed in the coating TiO_2 layer after heating of EPS-TiO_2 at 140 °C, which slowed down diffusion of the ethylene gas to the active surface. EPS spheres coating by bilayer SiO_2–TiO_2 are the promising material for application as the photocatalytic bed in the fluidized bed reactor.

Material and methods

Materials

Expanded polystyrene spheres (EPS, average size 1.07 ± 0.182 mm; Tehong Internation, China), tetraethyl orthosilicate (TEOS, Sigma-Aldrich, 98%), ammonia solution (Chempur, 30%), ethanol (Stanlab, 96%), hexadecyltrimethylammonium bromide (CTAB Merck, pure), hydrochloric acid (Stanlab, 35–38%), tetraisopropyl orthotitanate (TIPOT, Sigma-Aldrich, 97%), fumed silica Aerosil OX50 (Evonik), TiO_2 P25 (Evonik) were used as received without further purification, anatase type TiO_2 (Ar400) prepared in the laboratory—preparation method of sample was described in details in the previous paper [38]. The XRD spectra of the materials used as coatings in PS-based composites are shown in Fig. S13 (Supplementary materials). TiO_2 Ar400 and P25 contain a predominantly rutile phase, while sol–gel TiO_2 is amorphous. SiO_2 Aerosil OX50 have amorphic structure.

Coating of EPS with SiO_2 by a sol–gel method

EPS were coated using the Stöber method [40]. For this purpose, 0.8 g of EPS spheres were added into a mixture of 60 ml of ethanol and 1–3 ml of 30 wt% ammonia solution. Such prepared mixture was stirred for 30 min at room temperature. Subsequently, 2 g of TEOS mixed with 30 ml of ethanol were added slowly and left for stirring at room temperature during 24 h. All the ingredients of the reactor were then transferred to the rotary evaporator, where the solvent was removed. The composites were dried at 70 °C for 24 h.

In the second method of EPS coating, the sol–gel method in an acidic environment was applied [16]. 0.8 g of EPS spheres were added into a mixture of 40 g of ethanol and 10 ml of water. The pH of the mixture was adjusted to 2.5 by HCl and then the reaction mixture was heated up to 60 °C. After that 3 g of TEOS in 10 g of ethanol was added dropwise. The reaction was carried out for 5 h under constant stirring. Subsequently evaporation of solvent took place in a rotary evaporator and residues were dried at 70 °C for 24 h.

In the next method of EPS coating, the sol–gel process was conducted at the presence of CTAB (cetyltrimethylammonium bromide) surfactant [41]. For this purpose, 0.32 g CTAB was added into a mixture of 39.5 g of ethanol and 1 ml of 30% ammonia. Then 0.2 g of polystyrene spheres were poured in the sol–gel solution, and all of this was mixed for 30 min. Subsequently 0.47 g TEOS dissolved in 5 g ethanol was added very slowly (from an addition funnel). The mixture was then stirred for 2 h at 35 °C. After that the solvent was removed in a rotary evaporator. The composites were dried at 70 °C for 24 h.

Coating of EPS and EPS-SiO_2 spheres with TiO_2

EPS-SiO_2 spheres were prepared from a sol–gel solution by the Stöber method described above. TiO_2 coating was realized by both sol–gel solution and impregnation form an aqueous suspension of crystallized TiO_2. In the sol–gel method the silica-coated EPS spheres were placed in a glass reactor filled with 50 ml of deionized water and remained under stirring. Then, 2 g of TIPOT diluted with 15 ml of isopropanol was added very slowly to the reaction mixture under constant stirring for 24 h. After this time, the reactor contents were transferred to a rotary evaporator and solvent was removed. The composites were dried at 70 °C for 24 h. The BET-specific surface area of the SiO_2 powders obtained was 40 m^2/g and their pore volume was 0.220 cm^3/g.

The second method of TiO_2 coating on the EPS and EPS-SiO_2 spheres was based on the impregnation of crystallized TiO_2 from an aqueous suspension. As a source of TiO_2, two samples were used, commercial P25 (Evonik) and the other one prepared in the laboratory marked as Ar400. Ar400 has a higher BET area (167 m^2/g) and pore volume (0.425 cm^3/g) compared to P25 (54 m^2/g and 0.153 cm^3/g, respectively). In addition, AR 400 is composed of 97% anatase and 3% rutile and the smaller crystallite size of anatase (15 nm), where P25 consists of 78% anatase and 22% rutile and crystallite size of anatase (21 nm). These materials also differ in zeta potential (P25 + 31 mV; Ar400 + 13 mV) and OH^- group content (1% for P25 and 4% for Ar400). Anatase type TiO_2 had higher surface area and exposed higher quantity of OH species.

For impregnation of TiO_2 on the EPS spheres, 0.3 g of TiO_2 and 100 ml of deionized water were placed in an ultrasonic bath for 10 min. Then, 0.8 g of EPS spheres were added to the titania suspension and all the mixture was moved to a rotary evaporator, where the water was evaporated. The composites were dried at 70 °C for 24 h.

Thermal treatment of core–shell composites

The prepared core–shell composites (EPS-SiO_2, EPS-TiO_2 and EPS-SiO_2–TiO_2) were thermally treated in order to increase the adhesion of coating material with EPS spheres. The heat-treatment process was carried out in a muffle furnace at various temperatures, in the range of 120–140 °C for 6 h.

Composite characteristics

EPS spheres before and after coating were characterized by various methods including: the scanning electron microscope (SEM) micrographs with EDS analyses, UV–Vis/DR spectroscopy, thermal gravimetry (TG), zeta potential measurement and particles size distribution. SEM/EDS images were obtained using an ultra-high-resolution field emission scanning electron microscope (UHR FE-SEM Hitachi SU8020, Tokyo, Japan).

UV–Vis spectra were recorded in the wavelength range from 190 to 500 nm using UV–Vis apparatus (Jasco 650) with horizontal integrating sphere (PIV-756). Band gap energies for both TiO_2 samples as powders and coating were determined using the modified Kubelka–Munk equation, with a baseline approach. This method was described in detail elsewhere [42].

TG analyses were carried out in the thermobalance (TG, Netzsch STA 449 C, Germany) under flow of synthetic air (99.999% pure, 30 ml/min). Applied temperature program was as follows: heating to 30 °C with 30 min standby, then heating to 600 °C with heating rate of 10 K/min. The sample weight used for TG analyses was approximately 5 mg. Each sample was analyzed 3 times and then the final result was averaged. The total weight was the sum of EPS, ash residues, SiO_2 and TiO_2 contents:

$$m_{total} = m_{EPS} + m_{ash} + m_{SiO2} + m_{TiO2}$$

Therefore, the percentage of each component was calculated by simply subtracting it from the total weight loss.

Both the zeta potential and particles size distribution of SiO_2 and TiO_2 powders were measured in Zetasizer Nano ZS analyzer (Malvern, UK). Analyses were performed simply by preparing a dispersion of the sample in deionized water (0.4 g/l).

XRD measurements were performed using a diffractometer (PANanalytical, The Netherlands) equipped with a Cu X-ray source, $\lambda = 0.154439$ nm. The measurements covered the 2θ range of 20°–90° with a step size of 0.013. A voltage of 35 kV and a current of 30 mA were applied during the measurements.

Photocurrent response measurements and electrochemical impedance spectroscopy (EIS) were carried out using an Autolab PGSTAT302N potentiostat in a 3-electrode test cell with a platinum wire as counter electrode and a saturated calomel electrode as reference. The detailed procedure was described elsewhere [43].

Textural properties were determined on the basis of nitrogen sorption at -196 °C (QUADRASORB evo Gas Sorption Surface Area and Pore Size Analyzer). Prior to the sorption measurements all samples were outgassed at 250 °C for at least 20 h. The specific surface area was calculated on the basis of the Brunauer–Emmett–Teller (BET) equation and multi-point method.

Photocatalytic decomposition of ethylene

The photocatalytic decomposition of ethylene was carried out in the quartz photoreactor, which was located in the thermostatic chamber set at 25 °C. Tested samples were immobilized on the set of 6 glass plates (24 cm^2 of total plates area), which were afterwards put inside the quartz photoreactor. The model ethylene gas with a concentration of 50 ppm was supplied to the photoreactor from the bottle (80% N_2, 20% O_2, 50 ppm ethylene). The flow rate was controlled with a flow meter and was set at 20 ml/min. Ethylene gas was flowing through the photoreactor and then was directed to the gas chromatograph (SRI 8610C with the FID detector), where measurements were carried out at 15-min intervals. The quartz tube was surrounded with the set of 3 ring-shaped UV lamps as a light source, emitting light from the UV-A range (radiation intensity of 25.7 W/m^2, measured via HD2102.1 Photo-radiometer, TEST-THERM, Poland). The scheme of the system is illustrated in Fig. S14 (Supplementary materials).

The emission spectrum of the UV lamps utilized in photocatalytic tests was measured via USB4000 Fiber Optic Spectrometer (OceanOptics, USA) and is illustrated in Fig. S15 (Supplementary materials).

Acknowledgments

Not applicable.

Author contributions

P.M.: conceptualization, investigation, data curation, formal analysis, methodology, writing-original draft, writing-review and editing, visualization; P.R.. conceptualization, investigation, data curation, formal analysis, methodology, writing-original draft, writing-review and editing, visualization; B.T.: conceptualization, investigation, data curation, formal analysis, methodology, writing-original draft, writing-review and editing, project administration.

Funding

This work was supported by National Science Centre, Poland [Grant nr 2020/39/B/ST8/01514].

Data availability

The raw/processed data required to reproduce this research are available from the corresponding author upon reasonable request.

Declarations

Conflict of interest On behalf of all authors, the corresponding author states that there is no conflict of interest.

Supplementary Information

The online version contains supplementary material available at https://doi.org/10.1557/s43578-024-01319-3.

Open Access

References

1. H.P. Kuo, C.T. Wu, R.C. Hsu, Continuous reduction of toluene vapours from the contaminated gas stream in a fluidised bed photoreactor. Powder Technol. **195**(1), 50 (2009). https://doi.org/10.1016/j.powtec.2009.05.010
2. H.P. Kuo, C.T. Wu, R.C. Hsu, Continuous toluene vapour photocatalytic deduction in a multi-stage fluidised bed. Powder Technol. **210**(3), 225 (2011). https://doi.org/10.1016/j.powtec.2011.03.022
3. G.J. Rincón, E.J. La Motta, A fluidized-bed reactor for the photocatalytic mineralization of phenol on TiO_2-coated silica gel.

Heliyon **5**(6), e01966 (2019). https://doi.org/10.1016/j.heliyon.2019.e01966

4. R.L. Pozzo, J.L. Giombi, M.A. Baltanás, A.E. Cassano, Performance in a fluidized bed reactor of photocatalysts immobilized onto inert supports. Catal. Today **62**(2–3), 175 (2000). https://doi.org/10.1016/S0920-5861(00)00419-3
5. N. Pronina, D. Klauson, A. Moiseev, J. Deubener, M. Krichevskaya, Titanium dioxide sol–gel-coated expanded clay granules for use in photocatalytic fluidized-bed reactor. Appl. Catal. B **178**, 117 (2015). https://doi.org/10.1016/j.apcatb.2014.10.006
6. S. Li, M. Cai, Y. Liu, C. Wang, R. Yan, X. Chen, Constructing Cd0.5Zn0.5S/Bi_2WO_6 S-scheme heterojunction for boosted photocatalytic antibiotic oxidation and Cr(VI) reduction. Adv. Powder Mater. **2**(1), 100073 (2023). https://doi.org/10.1016/j.apmate.2022.100073
7. S. Li, M. Cai, C. Wang, Y. Liu, Ta3N5/CdS core-shell S-scheme heterojunction nanofibers for efficient photocatalytic removal of antibiotic tetracycline and Cr(VI): performance and mechanism insights. Adv. Fiber Mater. **5**(3), 994 (2023). https://doi.org/10.1007/s42765-022-00253-5
8. A. Kierys, R. Zaleski, M. Grochowicz, M. Gorgol, A. Sienkiewicz, Polymer–mesoporous silica composites for drug release systems. Microporous Mesoporous Mater. **294**, 109881 (2020). https://doi.org/10.1016/j.micromeso.2019.109881
9. C.W. Chen, T. Serizawa, M. Akashi, Preparation of platinum colloids on polystyrene nanospheres and their catalytic properties in hydrogenation. Chem. Mater. **11**(5), 1381 (1999). https://doi.org/10.1021/cm9900047
10. O. Siiman, A. Burshteyn, Preparation, microscopy, and flow cytometry with excitation into surface plasmon resonance bands of gold or silver nanoparticles on aminodextran-coated polystyrene beads. J. Phys. Chem. B **104**(42), 9795 (2000). https://doi.org/10.1021/jp000255z
11. X. Xu, L. Zhang, S. Zhang, Y. Wang, B. Liu, Y. Ren, Core–shell structured phenolic polymer@TiO_2 nanosphere with enhanced visible-light photocatalytic efficiency. Nanomaterials **10**(3), 467 (2020). https://doi.org/10.3390/nano10030467
12. I. Park, S.H. Ko, Y.S. An, K.H. Choi, H. Chun, S. Lee, G. Kim, Monodisperse polystyrene-silica core-shell particles and silica hollow spheres prepared by the Stöber method. J. Nanosci. Nanotechnol. **9**(12), 7224 (2009). https://doi.org/10.1166/jnn.2009.1636
13. Y. Hotta, P.C.A. Alberius, L. Bergström, Coated polystyrene particles as templates for ordered macroporous silica structures with controlled wall thickness. J. Mater. Chem. **13**(3), 496 (2003). https://doi.org/10.1039/b208795m
14. X. Cao, G. Pan, P. Huang, D. Guo, G. Xie, Silica-coated core-shell structured polystyrene nanospheres and their size-dependent mechanical properties. Langmuir **33**(33), 8225 (2017). https://doi.org/10.1021/acs.langmuir.7b01777
15. D. Sarma, K. Gawlitza, K. Rurack, Polystyrene core-silica shell particles with defined nanoarchitectures as a versatile platform for suspension array technology. Langmuir **32**(15), 3717 (2016). https://doi.org/10.1021/acs.langmuir.6b00373
16. M. Chen, S. Zhou, L. Wu, S. Xie, Y. Chen, Preparation of silica-coated polystyrene hybrid spherical colloids. Macromol. Chem. Phys. **206**(18), 1896 (2005). https://doi.org/10.1002/macp.200500200
17. Y. Han, Z. Lu, Z. Teng, J. Liang, Z. Guo, D. Wang, M.Y. Han, W. Yang, Unraveling the growth mechanism of silica particles in the stöber method: In situ seeded growth model. Langmuir **33**(23), 5879 (2017). https://doi.org/10.1021/acs.langmuir.7b01140
18. C. Tobias, E. Climent, K. Gawlitza, K. Rurack, Polystyrene microparticles with convergently grown mesoporous silica shells as a promising tool for multiplexed bioanalytical assays. ACS Appl. Mater. Interfaces **13**(1), 207 (2021). https://doi.org/10.1021/acsami.0c17940
19. H. Sertchook, D. Avnir, Submicron silica/polystyrene composite particles prepared by a one-step sol-gel process. Chem. Mater. **15**(8), 1690 (2003). https://doi.org/10.1021/cm020980h
20. Y.B. Zhang, X.F. Qian, H.A. Xi, J. Yin, Z.K. Zhu, Preparation of polystyrene core-mesoporous silica nanoparticles shell composite. Mater. Lett. **58**(1–2), 222 (2004). https://doi.org/10.1016/S0167-577X(03)00449-X
21. T. Hueckel, S. Sacanna, Mix-and-melt colloidal engineering. ACS Nano **12**(4), 3533 (2018). https://doi.org/10.1021/acsnano.8b00521
22. H. Zou, S. Wu, J. Shen, Polymer/silica nanocomposites: preparation, characterization, properties, and applications. Chem. Rev. **108**(9), 3893 (2008). https://doi.org/10.1021/cr068035q
23. I. Altin, M. Sökmen, Preparation of TiO_2-polystyrene photocatalyst from waste material and its usability for removal of various pollutants. Appl. Catal. B **144**, 694 (2014). https://doi.org/10.1016/j.apcatb.2013.06.014
24. S.H. Othman, N.R. Abd Salam, N. Zainal, R. Kadir Basha, R.A. Talib, Antimicrobial activity of TiO_2 nanoparticle-coated film for potential food packaging applications. Int. J. Photoenergy (2014). https://doi.org/10.1155/2014/945930
25. C. Graf, D.L.J. Vossen, A. Imhof, A. Van Blaaderen, A general method to coat colloidal particles with silica. Langmuir **19**(17), 6693 (2003). https://doi.org/10.1021/la0347859
26. K.G. de Castro Monsores, A.O. da Silva, S. de Sant'Ana Oliveira, R.P. Weber, P.F. Filho, S.N. Monteiro, Influence of ultraviolet radiation on polystyrene. J. Mater. Res. Technol. **13**, 359 (2021). https://doi.org/10.1016/j.jmrt.2021.04.035
27. S. Varnagiris, S. Tuckute, M. Lelis, D. Milcius, SiO_2 films as heat resistant layers for protection of expandable polystyrene foam from flame torch–induced heat. J. Thermoplast. Compos. Mater. **31**(5), 657 (2018). https://doi.org/10.1177/0892705717718238

28. S. Guruvenket, G.M. Rao, M. Komath, A.M. Raichur, Plasma surface modification of polystyrene and polyethylene. Appl. Surf. Sci. **236**(1–4), 278 (2004). https://doi.org/10.1016/j.apsusc.2004.04.033
29. Y. Ai, D. Wei, Preparation of hydrophilic polystyrene microspheres with casein molecules on the surface. J. Macromol. Sci. Part A **45**(6), 456 (2008). https://doi.org/10.1080/10601320801977731
30. Z. Wang, Y. Huang, S. Li, H. Xu, M.B. Linder, M. Qiao, Hydrophilic modification of polystyrene with hydrophobin for time-resolved immunofluorometric assay. Biosens. Bioelectron. **26**(3), 1074 (2010). https://doi.org/10.1016/j.bios.2010.08.059
31. S. Varnagiris, D. Girdzevicius, M. Urbonavicius, D. Milcius, Incorporation of SiO_2 and TiO_2 additives into expanded polystyrene foam using physical vapour deposition technique. Energy Procedia **128**, 525 (2017). https://doi.org/10.1016/j.egypro.2017.09.073
32. Y.J. Lee, C.G. Lee, J.K. Kang, S.J. Park, P.J.J. Alvarez, Simple preparation method for Styrofoam-TiO_2 composites and their photocatalytic application for dye oxidation and Cr(vi) reduction in industrial wastewater. Environ. Sci. Water Res. Technol. **7**(1), 222 (2021). https://doi.org/10.1039/d0ew00787k
33. J.C. Joo, G.Y. Kim, C.H. Ahn, S. Lee, J.-R. Park, J.K. Kim, J.-M. Oh, Application of titanium dioxide (TiO_2)-embedded buoyant photocatalyst balls using expanded polystyrene. J. Nanosci. Nanotechnol. **19**(2), 1151 (2018). https://doi.org/10.1166/jnn.2019.15936
34. J.C. Joo, S. Lee, C.H. Ahn, I. Lee, Z. Liu, J.-R. Park, Development of titanium dioxide (TiO_2)-immobilized buoyant photocatalyst balls using expanded polystyrene (EPS). Ecol. Resilient Infrastruct. **3**(4), 215 (2016). https://doi.org/10.17820/eri.2016.3.4.215
35. S. Sikandar Shah, I. Ahmad, M. Ishaq, Degradation study of used polystyrene with UV irradiation. Adv. Mater. Sci. **2**(3), 1 (2017). https://doi.org/10.15761/ams.1000130
36. I. Dundar, A. Mere, V. Mikli, M. Krunks, I.O. Acik, Thickness effect on photocatalytic activity of TiO_2 thin films fabricated by ultrasonic spray pyrolysis. Catalysts **10**(9), 1 (2020). https://doi.org/10.3390/catal10091058
37. V.R. Sastri, Commodity thermoplastics. Plast. Med. Devices **73**, 325–335 (2010). https://doi.org/10.1016/b978-0-8155-2027-6.10006-6
38. P. Rychtowski, B. Tryba, A. Skrzypska, P. Felczak, J. Sreńscek-Nazzal, R.J. Wróbel, H. Nishiguchi, M. Toyoda, Role of the hydroxyl groups coordinated toTiO_2 surface on the photocatalytic decomposition of ethylene at different ambient conditions. Catalysts **12**(4), 386 (2022). https://doi.org/10.3390/catal12040386
39. D.-R. Park, J. Zhang, K. Ikeue, H. Yamashita, M. Anpo, Photocatalytic oxidation of ethylene to CO_2 and H_2O on ultrafine powdered TiO_2 photocatalysts in the presence of O_2 and H_2O. J. Catal. **185**(1), 114 (1999). https://doi.org/10.1006/jcat.1999.2472
40. W. Chen, C. Takai, H.R. Khosroshahi, M. Fuji, T. Shirai, Surfactant-free fabrication of SiO_2-coated negatively charged polymer beads and monodisperse hollow SiO_2 particles. Colloids Surf. A **481**, 375 (2015). https://doi.org/10.1016/j.colsurfa.2015.06.008
41. Y. Chen, J. Qin, Y. Wang, Z. Li, Core/shell composites with polystyrene cores and meso-silica shells as abrasives for improved chemical mechanical polishing behavior. J. Nanoparticle Res. **17**(9), 363 (2015). https://doi.org/10.1007/s11051-015-3172-5
42. P. Makuła, M. Pacia, W. Macyk, How to correctly determine the band gap energy of modified semiconductor photocatalysts based on UV-Vis spectra. J. Phys. Chem. Lett. **9**(23), 6814 (2018). https://doi.org/10.1021/acs.jpclett.8b02892
43. P. Rychtowski, B. Tryba, D. Baranowska, B. Zielińska, H. Nishiguchi, M. Toyoda, Hydrogen evolution on the reduced TiO_2 under simulated solar lamp. Catal. Today **423**, 113989 (2023). https://doi.org/10.1016/j.cattod.2022.12.020